Spectrochimica Acta Part B: Atomic Spectroscopy 218 (2024) 106960

Contents lists available at ScienceDirect

Spectrochimica Acta Part B: Atomic Spectroscopy

journal homepage: www.elsevier.com/locate/sab

# LIBS as diagnostics of analytical chemistry for surface mapping of complex mixed samples simulating debris inside the TEPCO's Fukushima Daiichi Nuclear Power Plant (FDNPS) reactor cores

S. Almaviva [a,*], T. Karino [b], K. Akaoka [b], Ikuo Wakaida [b]

[a] ENEA, Italian National Agency for New Technologies, Environment and Sustainable Economic Development, Via E. Fermi, 45, 00040 Frascati, Italy
[b] Collaborative Laboratories for Advanced Decommissioning Science, Japan Atomic Energy Agency, 790-1 Motooka, Tomioka, Fukushima 979-1151, Japan

ARTICLE INFO

*Keywords:*
LIBS imaging
Nuclear debris analysis
Chemical maps

ABSTRACT

The Nuclear Energy Agency (NEA) launched the Nuclear Education, Skills and Technology (NEST) Framework to pursue careers in the nuclear field, by exposing researcher working on these topics to international challenging project of real-world issue and by transferring the knowledge and expertise accumulated in the current generation to them through hands-on training.

In this framework the 2022 edition of the NEST project offered a training educational period at the Collaborative Laboratories for Advanced Decommissioning (CLADS) located at Tomioka, Futaba District, in the Fukushima prefecture (Japan).

Among the research sectors active at CLADS there is the application and development of the LIBS technique as diagnostics of analytical chemistry aiming at characterizing the debris inside the Tokyo Electric Power Company (TEPCO)'s FDNPS reactor cores after the tsunami of March 2011, which destroyed three of the six reactors of the plant. These debris need to be chemically characterized with techniques suitable to be implemented in compact, remote and radiation resistant devices, due to the residual radioactivity of the cores. The present study shows the results in realizing chemical bi-dimensional maps of samples in the form of compressed tablets of mixed oxides, with a complex distribution and concentration of chemicals simulating these debris. The results allowed to create detailed maps of the samples, with spatial resolution down to 0.5 mm and an excellent correspondence between the real spatial distribution of the materials and that reconstructed by LIBS.

Moreover, it was found a good correspondence between the nominal concentration of the chemicals and the concentration estimated by using LIBS.

This study shows the potentialities of LIBS in the realization of chemical maps on samples of interest for FDNPS, providing multi-elemental images of the samples under analysis.

## 1. Introduction

The Fukushima Daichi nuclear accident occurred at the FDNPS, located in Naraha, Fukushima Prefecture, on the east coast of Japan. The triggering cause was the Tōhoku earthquake and tsunami of 11 March 2011 with an earthquake of approximately 9 degrees on the Richter scale, whose epicenter was located at 130 km offshore the city of Sendai, in Miyagi prefecture, on the eastern coast of Honshu Island and about 180 km from the plant [1]. Such a powerful earthquake had never been recorded in Japan's history until then [2].

During the earthquake, the plant's anti-seismic safety system shut down all the reactors and, in absence of electric power, the emergency electrical generators were immediately activated, providing the necessary energy to allow the normal functioning of the cooling systems.

However, after about 40–50 min, the plant was reached by the tsunami wave, about 15 m high, generated by the earthquake, which overcame the anti-tsunami protections of the plant and flooded it [1]. The tsunami destroyed the emergency generators that powered the cooling systems of reactors 1, 2 and 3. This caused an electrical blackout and a shutdown of the cooling systems in these reactors, causing the uncontrolled heating of the nuclear fuel rods in the reactor's pressure vessels (RPVs). As a result, the water used for cooling the nuclear fuel rods started to boil and vaporize, increasing pressure inside the RPVs.

A series of chemical reactions favored the electrolysis of the water,

* Corresponding author.
*E-mail address:* salvatore.almaviva@ena.it (S. Almaviva).

https://doi.org/10.1016/j.sab.2024.106960
Received 30 January 2024; Received in revised form 26 May 2024; Accepted 1 June 2024
Available online 3 June 2024

generating hydrogen gas which exploded in contact with the air [1,3]. Explosions of this type occurred in the reactors between 12 and 15 March and the fuel rods partially melted. The explosions destroyed the upper structures of two of the three damaged reactor buildings [3] and a heterogeneous compound (corium), consisting of molten nuclear fuel, mixed with various structural materials in the RPVs and in the primary containment vessels (PCVs) was formed [3–4]. To date, due to the high levels of radiation dose, the internal inspection of the RPVs and PCVs of the three units with human personnel is impossible and inspections have been carried out only by using robotic devices, to measure residual doses of radiation or acquire images of the current state of the inner parts of the cores. Therefore, the data currently available on the composition and distribution of debris, corium and residual nuclear fuel are based on calculations codes designed to predict the behavior of reactor systems during normal and accident conditions [4], although a detailed knowledge of these data is of paramount importance for deciding further strategies and phases of dismantling the three units.

To characterize the chemical composition of the materials inside RPVs and PCVs it is therefore necessary to develop up-to-date diagnostics, capable of working in real time and suitable to be implemented in radiation resistant devices. Among the eligible diagnostics, LIBS is a valid candidate for this purpose for several reasons.

Indeed, LIBS can provide the simultaneous detection of all the chemical elements [5] and, in some cases, the detection of different isotopes of the same element [6]. The sensitivity of the LIBS technique can reach trace levels, down to ppm [5,7] and no sample preparation, manipulation or alteration is strictly required. The technique is, in principle, only micro-destructive (only few micrograms of the sample are generally needed), offering the possibility to preserve the sample for further, complementary analyses.

Moreover, LIBS has depth profiling capabilities, i.e., it is possible to chemically characterize in-depth the samples by applying multiple laser shots in the same point [8]. LIBS can be also used for semi-quantitative or quantitative analyses of the composition of the sample [9–11]. Finally, from a technologically point of view, compact light, operating remotely LIBS systems are nowadays available on the market or can be designed for specific purposes [12], without personnel in close proximity to the target materials and giving results in real time.

LIBS imaging is currently under strong development, with an increase in the number of both published articles and innovative applications during the last few years. Indeed this methodology is becoming increasingly mature, and it is currently a good candidate to become a reference approach for the spatially resolved elemental characterization of different types of samples, metallic or non-metallic, with micrometric resolution and sensitivity of the order of ppm [13–16].

The technique has been already used in nuclear industry [6,17–19], for example to monitor and analyze different nuclear materials [19]. Since most of the measurements in the nuclear industry are conducted under various radiation environments, Wang et al. [20] performed a multi-elemental mapping of rare earth elements in nuclear waste glass–ceramic using micro-LIBS with 10 μm spatial resolution, investigating the long-term fractionation behavior of Mo, Ca, Sr, Al, Fe and Zr and rare-earth elements such as Eu, Nd, Pr and La on a Mo-rich nuclear waste glass-ceramic.

Batsaikhan et al. [21] performed a two-dimensional LIBS elemental mapping of simulated debris of nuclear fuel from fission by applying chemometric methods, such as Principal Component Analysis and Multivariate Curve Resolution-Alternative Least Square methods, obtaining the spatial and spectral information regarding each constituent within the simulated sample.

In the present work, the LIBS technique is applied to perform elemental surface mapping and semi-quantitative compositional analysis of complex samples simulating nuclear debris inside the FDNPS reactor's cores. Indeed, LIBS has been already identified as a powerful analytical technique in various fields providing reliable chemical maps and quantitative measurements [22]. The purpose of the present study is to demonstrate the reliability of this procedure for the characterization of nuclear materials in the corium of FDNPS.

## 2. Materials and methods

### 2.1. Sample preparation

Ten samples were prepared in the form of compressed tablets of mixtures of oxides of different metals, specifically, $Fe_3O_4$, $Er_2O_3$, $Ho_2O_3$, $Gd_2O_3$ and $ZrO_2$ (Rare Metallic Co., LTD, Tokyo, Japan). Five of them, with a diameter of 10 mm and a thickness of 2 mm were used as reference samples composed only by the pure oxides and were realized by pressing the oxide powder at 16kN and heating them at temperatures between 1300 and 1600 K for 1–4.5 h, depending on the oxide. The other five tablets, with a diameter of 13.7 mm and a thickness of 1 mm represented the simulated debris and were prepared similarly to the reference samples, but with a complex surface distribution and concentration of the oxides, to simulate the expected heterogeneous composition of the debris inside the RPVs and PCVs of the three damaged units [4]. The choice of these materials was dictated by their use in fission technology. In particular, Fe is expected to be found as melted and oxidized material from the structural stainless steel of RPVs and PCVs, Zr as cladding materials of the fuel elements and fission products, Ho and Gd as neutron absorber in nuclear control rods [23,24] and Er as a burnable absorber in the fuel elements [25]. In Fig. 1 pictures and schemes of the five tablets, with spatial distribution and concentration of the different oxides reported to the right of each sample.

### 2.2. LIBS system

A schematic diagram of the experimental apparatus used in this study is fully illustrated elsewhere [21]. Here we want only summarize that it consists of a Nd:YAG pulsed laser source (ULTRA series, Quantel, USA) operating at 532 nm wavelength, max pulse energy 55 mJ, pulse duration 10 ns. The laser beam is focused through a series of optics on a three-axis micrometric stage inside an analysis chamber (LIBSpector, LTB, Germany) where the samples have been placed. Light form the laser-induced plasma is collected through an optical fiber, coupled with an Echelle spectrometer (ARYELLE-400, LTB Germany), equipped with an intensified CCD camera (ISTAR Andor, Northern Ireland), 16 bit dynamic range. The measurement range of the Aryelle spectrometer spans between 435 and 657 nm, with an average resolution of 11 pm. To map the surface of the sample, a pixel-by-pixel scanning procedure was adopted as schematized in Fig. 2, the energy of each laser pulse being 44 mJ, acquisition delay 3 μs, gate width 10 μs. These parameters have been chosen to optimize the signal-to-noise ratio (SNR) of the spectral data for a single laser shot released on the sample. Indeed, in the case of the present samples the thickness of the oxide layers were in the range of some hundreds micrometers and it was possible to apply multiple laser shots for each point of analysis, but, in a real sample the thickness of a single layer of oxide could be very small and a layer of material can be removed with a single laser shot. Therefore, we adopted these parameters to be able to carry out the surface mapping even applying a single laser shot, as done for the sample S5. Instead for the other samples 20 laser shots were released on the same point at repetition rate of 10 Hz, to further increase SNR. The stage moved along the two-horizontal axes with a pitch of 0.5 mm, through a home-made routine of the Sophy™ acquisition software, controlling both the stage and the laser and allowing to scan the sample with a pre-established pitch. Before releasing the sequence of 20 shots, this routine also optimizes the laser focus in the analysis point, resulting in an homogeneous scanning without loss of focus of the laser beam and all the laser spots with a diameter of about 250 μm on the samples surface. For each sample, the scanned area was rectangular and positioned to map all the oxides present in the samples at different concentrations. The overall surface of the mapped areas was about 9 × 10 mm (about 19 × 21 spots).

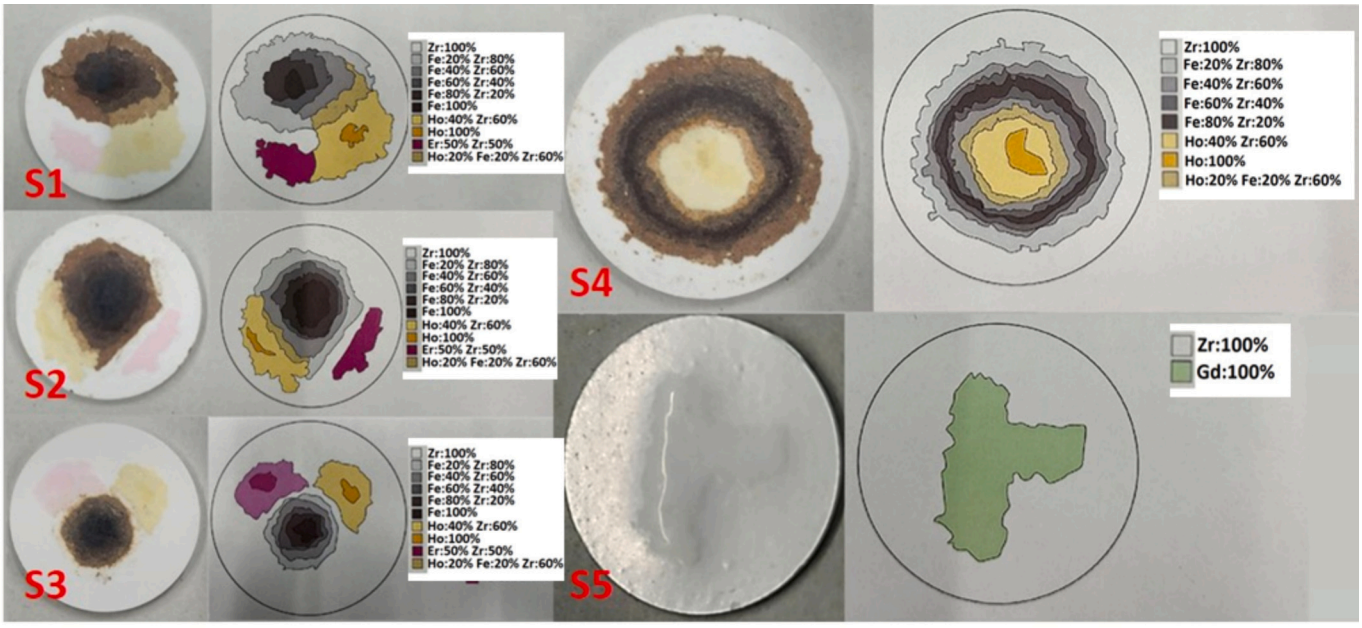


**Fig. 1.** Pictures of the five samples, labeled as S1 to S5 (to the left) together with the map of the spatial distribution and concentration of the different oxides (in the center). The colored squares on the right identify the oxides. Different shades of the same colour represent different concentrations of the same oxide. The concentrations of the oxides are in atomic percentage.

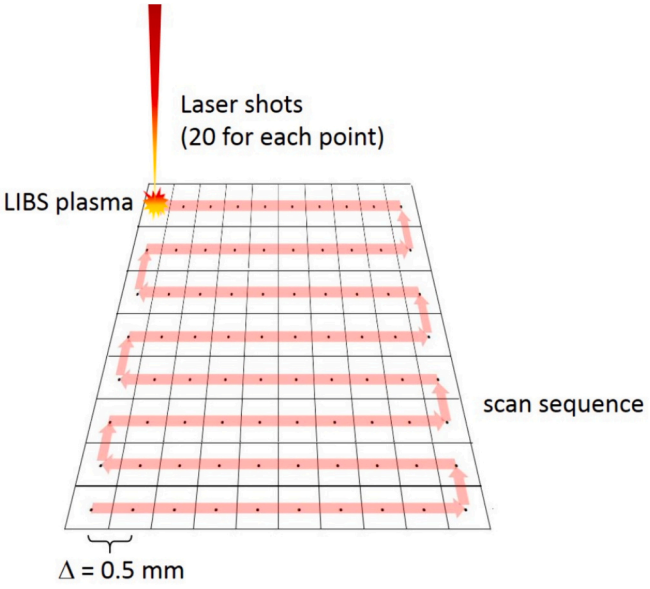


**Fig. 2.** Scheme of the applied LIBS scanning.

The S1 - S4 samples were scanned as described, the S5 sample was scanned by delivering a single laser shot instead of 20 consecutive ones, to limit the depth of the LIBS spot and perform an even more superficial mapping, although at the cost of a lower SNR. This slightly different approach was applied to verify the feasibility of a LIBS mapping by using a single laser shot of the debris, in case of a 3D complex distribution of materials [22,26].

## 3. Results and discussion

LIBS spectra of the reference samples, composed by the pure oxides, were used to find the peculiar and most evident spectral emissions of the oxides under analysis. Fig. 3 shows representative spectra of these oxides.

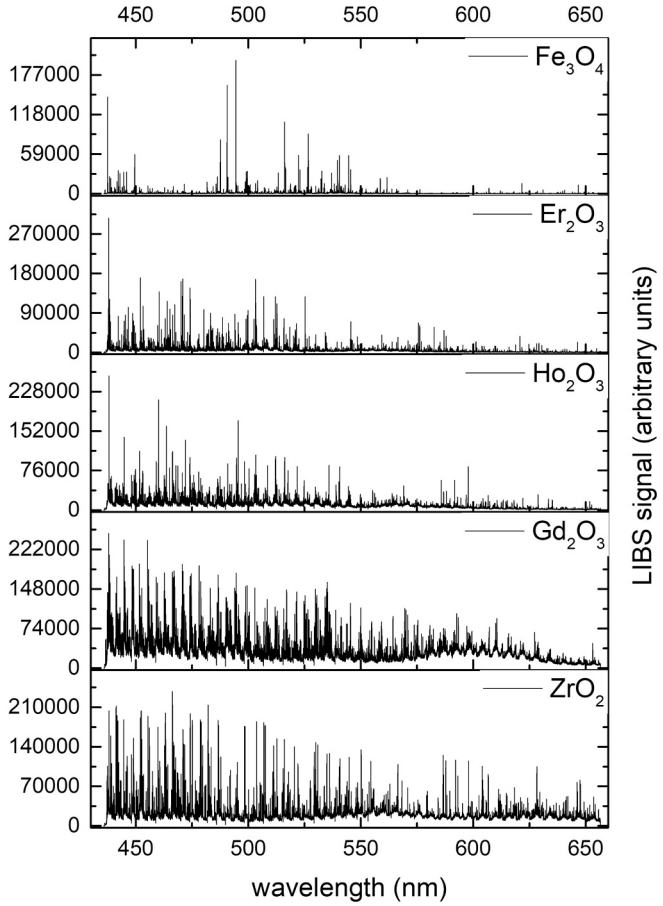


**Fig. 3.** LIBS spectra of the reference samples in the available spectral range.

These peculiar emission lines were selected based on the following requirements:

i) to be relatively free from interference from emission lines of other oxides.
ii) showing a high SNR
iii) with intensity proportional to the concentration of the relative species.

Despite the inherent richness and complexity of the LIBS spectra generated from the pure oxides and according to literature database of atomic emissions [27] the following lines have been identified, in accordance, as far as possible with the requirements specified above, considering that the pure oxides are extremely rich in spectral emissions throughout the entire spectral range: Er II at 451.94 nm, Fe I at 490.33 nm, Gd I at 437.86 nm, Ho II at 437.98 nm and Zr I at 482.43 nm, and reported for each element in Fig. 4a-e.

The spectral emission of Ho does not completely satisfy the requirements specified above, as it interferes with some spectral emissions of $Zr_2O_3$. However, this spectral line was chosen as a compromise solution because it had, in these complex matrices, a high SNR and linearity with the $Ho_2O_3$ concentration, well satysfing conditions ii) and iii) although conditions i) is only partially satisfied.

Finally, before carrying out the two-dimensional mapping, the linear correlation between the emission intensity and the concentration of the relative oxide was verified on many linear scans of the samples, in which the known concentration of the oxides changed significantly.

An example is shown in Fig. 5 (sample S1), where the intensity trend of the Zr, Fe, Er, Ho, emission lines along the thirteen horizontal scan was reported. Similar results for other linear scans justified the assumption that the line intensity for each element reliably correlates with concentrations of the oxides, opening the possibility of a semi-quantitative analysis of the relative concentration of the elements.

The semi-quantitative analysis was thus performed by re-normalizing the line intensity values from [0;100] according to the following formula:

$$C_{el} = \left( \frac{(I)_{\lambda(el)} - bgn(\lambda)}{Max(I)_{\lambda(el)} - bgn(\lambda)} \right) \times 100 \quad (1)$$

where $C_{el}$ is the concentration of the chemical element, $(I)_{\lambda(el)}$ is the peak intensity of the chosen emission lines for that element, $Max(I)_{\lambda(el)}$ is the peak intensity computed on the LIBS measurements of the pure oxide (where the concentration of the element is assumed to be 100%) and $bgn(\lambda)$ is the background signal acquired in a spectral region nearby the emission line ($\leq$ 0.15 nm far from the line), 5 pixels width ($\leq$ 55 pm), being free from other emission lines of the element or from their tails.

By applying this procedure, we obtained the two-dimensional concentration matrices for each element, each cell of these matrices representing the elemental concentration in the sampling points. The concentration maps are shown in Fig. 6, where different concentrations are represented by different colors, according to the relative reference bars.

The results of this study showed the capability of LIBS in mapping samples simulating fission debris with a inhomogeneous composition inside the three damaged units of FDNPS. The elemental maps showed an excellent correlation between the spatial distribution of the elements and that obtained with LIBS with sub-millimetric resolution. Each mapping required a scan time of approximately 30 min. Despite the spatial superposition of the various oxides, even in the case of the sample S5, to which only one laser shot was applied per scanning point, the surface maps are reliable, although the composition of the sample is

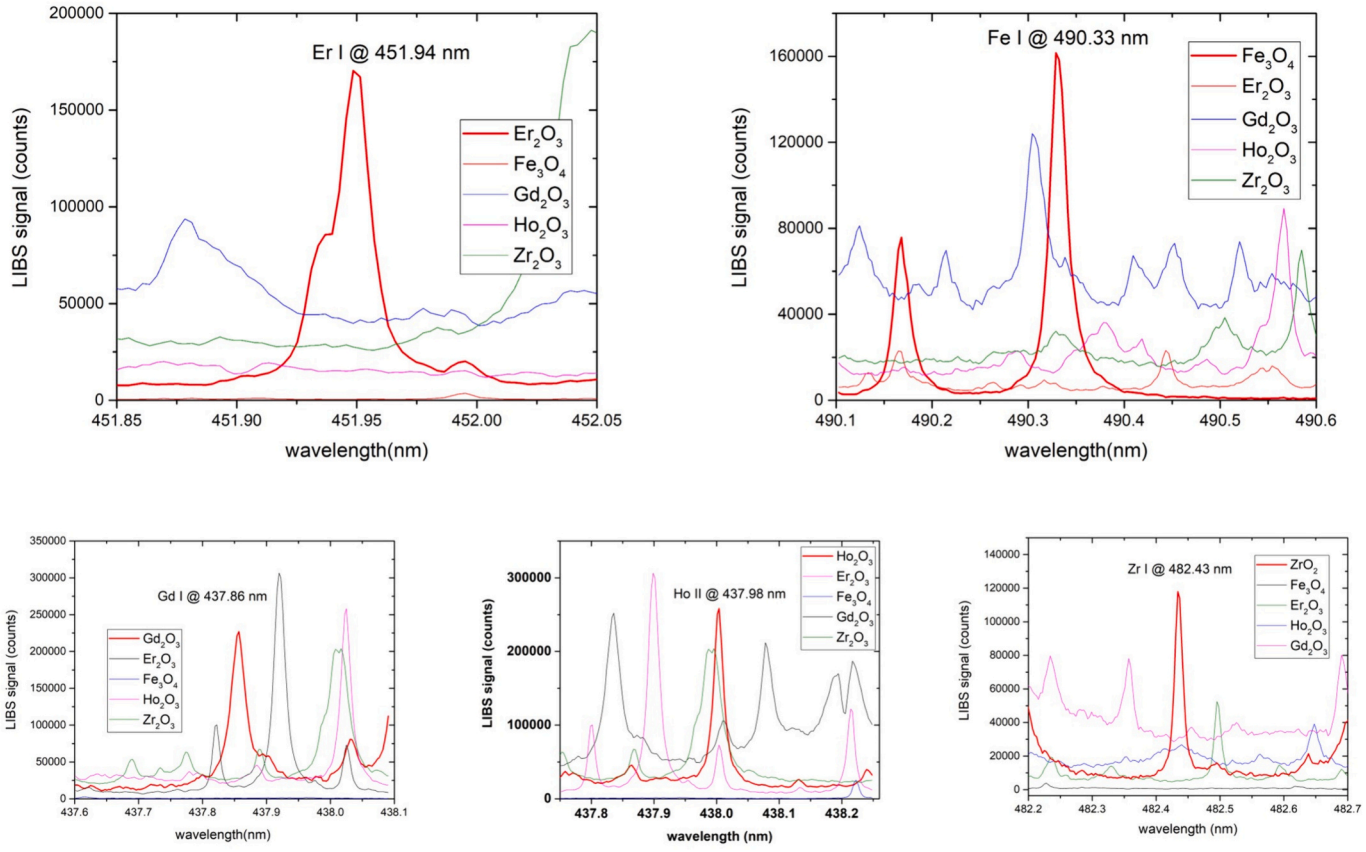


**Fig. 4.** Selected spectral windows of the LIBS spectra of the pure oxides displaying emission lines of Er (a), Fe (b), Gd (c), Ho (d) and Zr (e) (bold red lines), together with the spectra of the other oxides. (For interpretation of the references to colour in this figure legend, the reader is referred to the web version of this article.)

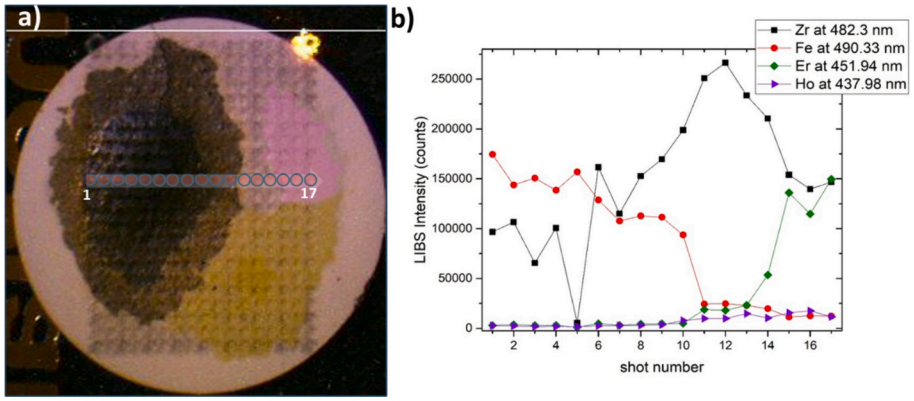


**Fig. 5.** a) Sample S1 after the LIBS scan. The thirteen horizontal scan is highlighted with pale red dots. Arrow and numbers indicate the scan direction. b) Trend of the intensities of the emission line of Fig. 4 for Zr, Fe, Er and Ho. (For interpretation of the references to colour in this figure legend, the reader is referred to the web version of this article.)

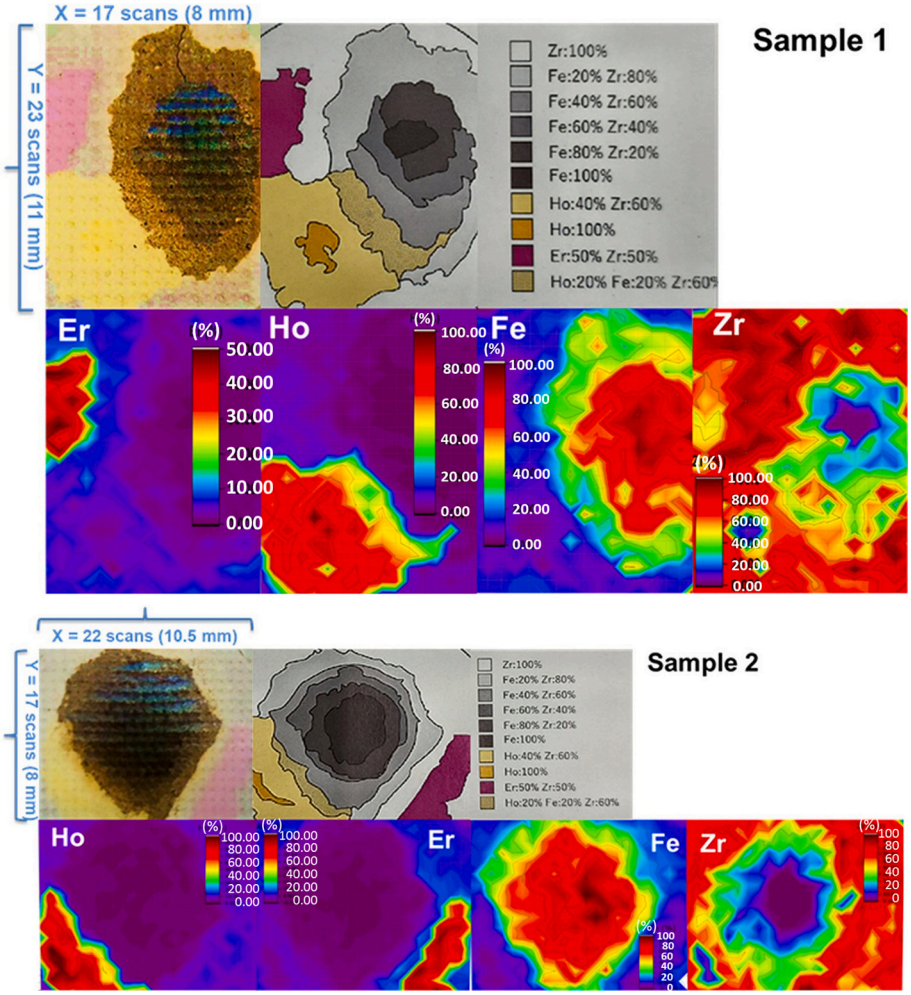


**Fig. 6.** Elemental maps by LIBS of the five samples. On the top of the figure of each sample is displayed: 1) the scanned area with the number of applied spots, 2) the spatial composition of the sample in the scanned area, 3) a calibration bar showing the concentration of the different oxides. At the bottom of the figure are displayed the LIBS elemental maps as follows: Er images at 451.94 nm, Fe images at 490.33 nm, Gd image at 437.86 nm, Ho images at 437.98 nm. The concentration bars display the minimum concentration in violet, corresponding to the background level and the maximum concentration in dark red. (For interpretation of the references to colour in this figure legend, the reader is referred to the web version of this article.)

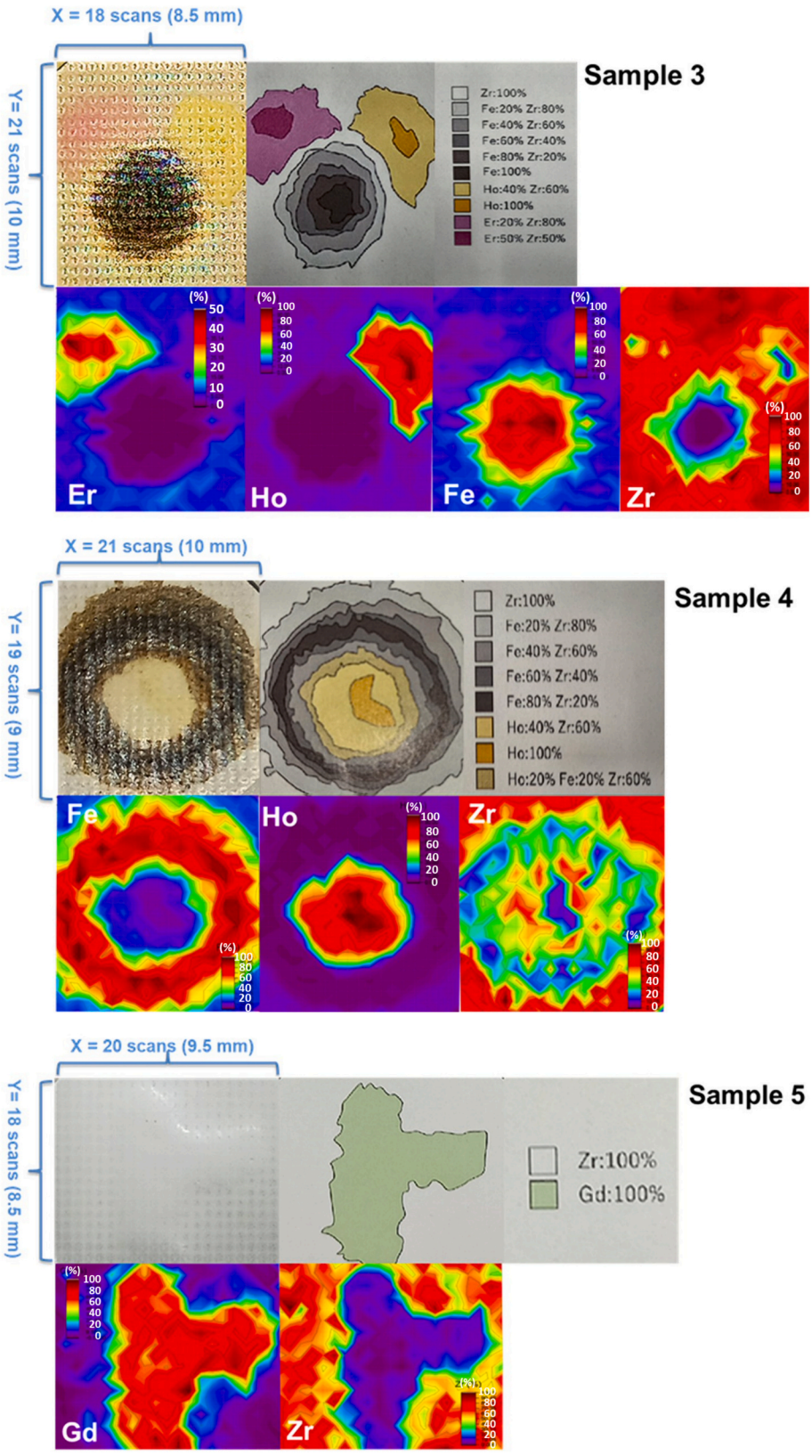


**Fig. 6.** (*continued*).

simplified, compared to the others. This last result, however, demonstrates that the proposed procedure could also be applied to carry out detailed 3D elemental mapping with axial resolution fixed to the depth of the LIBS spot induced by a single laser shot.

## 4. Conclusions

In this work, we applied LIBS in imaging mode to chemically characterize five samples simulating debris inside the damaged reactors of

FDNPS after the tsunami of March 2011.

The samples, in the form of pellets of mixed oxides, had a complex surface distribution, with variations in concentration for each oxide. They have been characterized with a detailed surface mapping, with a pitch of 0.5 mm and an area of about 9 × 10 mm (for a total of about 400 points per sample). Mapping of each element was based on preliminary LIBS measurements of the corresponding pure oxides as reference samples, to identify peculiar emission lines free from interference from emission lines of other elements and with a high SNR. Moreover, these spectral emissions exhibited a linear correlation between the peak intensity and the concentration of the relative species, representing a sort of "fingerprint" for those species.

The results showed an excellent correlation between the real spatial distribution of the oxides and that reconstructed by LIBS and a good correspondence between the nominal concentration of each element and the concentration obtained by LIBS. One of the samples, with a relatively simplified surface distribution of two oxides was mapped by delivering a single laser shot for each analysis point, instead of applying multiple shots. Even in this case, the maps were reliable and a good semi-quantitative estimation of the concentration of each element was obtained, although with a lower SNR. This result can be exploited for a 3D mapping of more complex samples, where the in-depth distribution of different compounds could be a complex superposition or interposition of different compounds, as in the case of real samples.

## CRediT authorship contribution statement

**S. Almaviva:** Writing – review & editing, Writing – original draft, Visualization, Methodology, Investigation, Formal analysis, Data curation, Conceptualization. **T. Karino:** Supervision, Software, Methodology. **K. Akaoka:** Supervision, Software, Methodology. **Ikuo Wakaida:** Supervision, Project administration, Methodology.

## Declaration of competing interest

The authors declare no conflict of interest.

## Data availability

Data will be made available on request.

## Acknowledgements

This study partly includes the results of NEST fellowship in CLADS/JAEA, funded by OECD/NEA and Japanese Government (MEXT).

## References

[1] https://world-nuclear.org/information-library/safety-and-security/safety-of-plants/fukushima-daiichi-accident.aspx.
[2] Japan Meteorological Agency, Information on the 2011 off the Pacific Coast of Tohoku Earthquake. http://www.jma.go.jp/jma/en/2011_Earthquake/Information_on_2011_Earthquake.html, 2015.
[3] B. Grambow, et al., Ten years after the NPP accident at Fukushima : review on fuel debris behavior in contact with water, J. Nucl. Sci. Technol. 59 (1) (2022) 1–24, https://doi.org/10.1080/00223131.2021.1966347.
[4] A. Nakayoshi, et al., Review of Fukushima Daiichi nuclear Power Station debris endstate location in OECD/NEA preparatory study on analysis of fuel debris (PreADES) project, Nucl. Eng. Des. 369 (2020) 110857, 15, https://doi.org/10.1016/j.nucengdes.2020.110857.
[5] D.A. Cremers, L.J. Radziemski, Handbook of Laser-Induced Breakdown Spectroscopy, 2nd ed, John Wiley & Sons, 2013.
[6] M. Miyabe, et al., Laser ablation absorption spectroscopy for isotopic analysis of plutonium: spectroscopic properties and analytical performance, Spectrochim. Acta B 134 (2017) 42–51.
[7] Z.H. Khan, et al., Laser-induced breakdown spectroscopy (LIBS) for trace element detection: a review, Jou. Spectrosc. 2022 (2022) 25, https://doi.org/10.1155/2022/3887038.
[8] A. Królicka, A. Maj, G. Łój, Application of laser-induced breakdown spectroscopy for depth profiling of multilayer and graded materials, Materials (2023) 26, https://doi.org/10.3390/ma16206641, 16, 6641.
[9] S. Nisar, G. Dastgeer, M. Shafiq, M. Usman, Qualitative and semi-quantitative analysis of health-care pharmaceutical products using laser-induced breakdown spectroscopy, Jou. Pharmaceut. Anal. 9 (1) (2019) 20–24, https://doi.org/10.1016/j.jpha.2018.10.003.
[10] A. Ismaël, et al., In situ semi-quantitative analysis of polluted soils by laser-induced breakdown spectroscopy (LIBS), Appl. Spectrosc. 65 (2011) 467–473.
[11] J.A. Bolger, Semi-quantitative laser-induced breakdown spectroscopy for analysis of mineral Drill Core, Appl. Spectrosc. 54 (2) (2000) 181–189.
[12] J. Pedarnig, et al., Review of element analysis of industrial materials by in-line laser—induced breakdown spectroscopy (LIBS), Appl. Sci. 11(19), 9274 (2021) 46, https://doi.org/10.3390/app11199274.
[13] V. Motto-Ros, et al., LIBS-based imaging: recent advances and future directions, Spectroscopy 35 (2) (2020) 34–40.
[14] V. Gardette, et al., Laser-induced breakdown spectroscopy imaging for material and biomedical applications: recent advances and future perspectives, Anal. Chem. 95 (1) (2023) 49–69.
[15] A. Limbeck, et al., Methodology and applications of elemental mapping by laser induced breakdown spectroscopy, Anal. Chim. Acta 1147 (2021) 72–98.
[16] P. Janovszky, et al., Quantitative elemental mapping of biological tissues by laser-induced breakdown spectroscopy using matrix recognition, Sci. Rep. 13, 10089 (2023) 10.
[17] A. Sarkar, S. Mukherjee, M. Singh, Determination of the uranium elemental concentration in molten salt fuel using laser-induced breakdown spectroscopy with partial least squares-artificial neural network hybrid models, Spectrochim. Acta B 187 (2022) 106329, 8.
[18] M. Singh, R.K. Misra, P.G. Jaison, C.P. Cuashik, A. Sarkar, Direct quantitative analysis of a cesium pencil in a simulated hot-cell using a remote-LIBS system equipped with a miniature collimator, Jou. Anal. At. Spectrom. 34 (2019) 1910–1918.
[19] W. Jian, et al., Progress of laser-induced breakdown spectroscopy in nuclear industry applications, Jou. Phys D: Appl. Phys. 53 (2) (2020), https://doi.org/10.1088/1361-6463/ab477a.
[20] X. Wang, et al., Mapping of rare earth elements in nuclear waste glass–ceramic using micro laser-induced breakdown spectroscopy, Spectrochim. Acta B 87 (2013) 139–146, https://doi.org/10.1016/j.sab.2013.05.022.
[21] M. Batsaikhan, et al., Two-dimensional elemental mapping of simulated fuel debris using laser-induced breakdown spectroscopy, J. Nucl. Sci. Technol. (2024), https://doi.org/10.1080/00223131.2023.2255186.
[22] A. Limbeck, et al., Methodology and applications of elemental mapping by laser induced breakdown spectroscopy, Anal. Chim. Acta 1147 (2021) 72–98, https://doi.org/10.1016/j.aca.2020.12.054.
[23] K. Wang, et al., Recent Progress in Gd-containing materials for neutron shielding applications: a review, Materials 10;16 (12) (2023), https://doi.org/10.3390/ma16124305, 4305 (28 pp.).
[24] A.B. Smith, Fast-neutrons incident on holmium, Ann. Nucl. Energy 28 (17) (2001) 1745–1758, https://doi.org/10.1016/S0306-4549(01)00015-9.
[25] J.A. Evans, M.D. DeHart, K.D. Weaver, J.D.D. Keiser, Burnable absorbers in nuclear reactors – a review, Nucl. Eng. Des. 391 (2022) 21, https://doi.org/10.1016/j.nucengdes.2022.111726.
[26] M.P. Mateo, G. Nicolas, Mapping capability of linear correlation statistics for characterization of complex materials using Laser-induced breakdown spectroscopy, Anal. Chim. Acta 1227 (2022), https://doi.org/10.1016/j.aca.2022.340260, 340260, 7.
[27] W.F. Meggers, C.H. Corliss, B.F. Scribner, Tables of Spectral Lines Intensities Part I, Arranged by Elements, 2nd ed., US National Bureau of Standard, 1975.